



Constrained dynamics of the sole tryptophan in the third intracellular loop of the serotonin_{1A} receptor



Sreetama Pal^{b,c}, Ramdas Aute^a, Parijat Sarkar^a, Shroddha Bose^a, Mandar V. Deshmukh^a, Amitabha Chattopadhyay^{a,b,*}

^a CSIR-Centre for Cellular and Molecular Biology, Uppal Road, Hyderabad 500 007, India

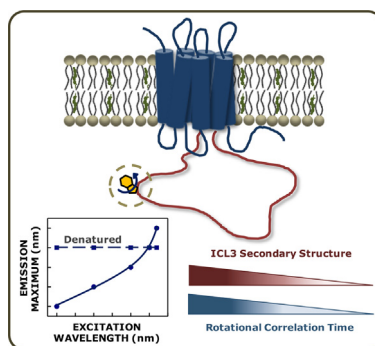
^b Academy of Scientific and Innovative Research, India

^c CSIR-Indian Institute of Chemical Technology, Uppal Road, Hyderabad 500 007, India

HIGHLIGHTS

- GPCR extramembranous regions are believed to be crucial for physiological functions.
- ICL3 of serotonin_{1A} receptor is implicated in G-protein coupling and activation.
- Sole tryptophan of serotonin_{1A} receptor ICL3 experiences constrained dynamics.
- This restricted dynamics is predominantly induced by peptide secondary structure.
- GPCR loop structure and dynamics may provide valuable insights into GPCR function.

GRAPHICAL ABSTRACT



ARTICLE INFO

Keywords:

ICL3
Constrained tryptophan dynamics
REES
Serotonin_{1A} receptor
GPCR

ABSTRACT

G protein-coupled receptors (GPCRs) are major signaling proteins in eukaryotic cells and are important drug targets. In spite of their role in GPCR function, the extramembranous regions of GPCRs are relatively less appreciated. The third intracellular loop (ICL3), which connects transmembrane helices V and VI, is important in this context since its crucial role in signaling has been documented for a number of GPCRs. Unfortunately, the structure of this loop is generally not visualized in x-ray crystallographic studies since this flexible loop is either stabilized using a monoclonal antibody or replaced with lysozyme. In this work, we expressed and purified the ICL3 region of the serotonin_{1A} receptor and monitored its motional restriction and organization utilizing red edge excitation shift (REES) of its sole tryptophan and circular dichroism (CD) spectroscopy. Our results show that the tryptophan in ICL3 exhibits REES of 4 nm, implying that it is localized in a restricted microenvironment. These results are further supported by wavelength-selective changes in fluorescence anisotropy and lifetime. This constrained dynamics was relaxed upon denaturation of the peptide, thereby suggesting the involvement of the peptide secondary structure in the observed motional restriction, as evident from CD spectroscopy and apparent rotational correlation time. To the best of our knowledge, these results constitute one of the first measurements of motional constraint in the ICL3 region of GPCRs. Our results are relevant in the context of the

Abbreviations: CD, circular dichroism; DMSO, dimethyl sulfoxide; DTT, dithiothreitol; GPCR, G protein-coupled receptor; ICL3, third intracellular loop; IPTG, isopropyl β-D-1-thiogalactopyranoside; PMSF, phenylmethylsulfonyl fluoride; REES, red edge excitation shift; TCSPC, time-correlated single photon counting

* Corresponding author at: CSIR-Centre for Cellular and Molecular Biology, Uppal Road, Hyderabad 500 007, India.

E-mail address: amit@ccmb.res.in (A. Chattopadhyay).

<https://doi.org/10.1016/j.bpc.2018.05.008>

Received 1 May 2018; Received in revised form 24 May 2018; Accepted 27 May 2018

Available online 01 June 2018

0301-4622/ © 2018 Elsevier B.V. All rights reserved.

reported intrinsically disordered nature of ICL3 and its role in providing functional diversity to GPCRs due to conformational plasticity.

1. Introduction

G protein-coupled receptors (GPCRs) are a family of seven transmembrane domain proteins that allow the exterior of the cell to communicate with the cellular interior [1–3]. In molecular terms, signaling carried out by GPCRs involves their activation by ligands present in the extracellular environment, followed by the transduction of signals to the interior of the cell through concerted conformational changes in their transmembrane domain. This could imply that various domains in GPCRs act in a cooperative fashion for carrying out signal transduction. GPCRs act as highly versatile and dynamic membrane sensors and mediate cellular responses to a diverse variety of stimuli in several physiological processes. As a consequence of diverse signaling by GPCRs, they have emerged as major drug targets in all clinical areas [4, 5].

Serotonin receptors represent a major class of GPCRs involved in brain function [6, 7]. These receptors play a crucial role in the generation and modulation of cognitive and behavioral functions. Malfunctioning of serotonergic systems is implicated in disorders such as depression, anxiety, schizophrenia, obsessive compulsive disorder and migraine. According to the present classification, there are 16 subtypes of serotonin receptors [8]. The serotonin_{1A} receptor is an important member of this family due to a number of reasons [9] and serves as an important target in drug discovery for neuropsychiatric disorders and cancer [8, 10]. Previous work from our laboratory has shown the crucial role of membrane cholesterol [11–13] and sphingolipids [13, 14] in the function of the serotonin_{1A} receptor.

Typically, GPCRs consist of seven transmembrane domains (helices) interconnected by several extracellular and intracellular loops. Since GPCRs have odd number of membrane passes, the N- and C-termini are located on opposite sides of the membrane (see Fig. 1). Most of the focus on GPCRs till date has been centered on the transmembrane helices. This is in spite of the fact that the extramembranous regions of GPCRs have been reported to have important functions for cellular signaling and desensitization. For example, the third intracellular loop (ICL3), which connects transmembrane helices V and VI, has been reported to be crucial for function [16–20] and dynamics [21, 22] of a number of GPCRs. Yet, this flexible loop was either stabilized using a monoclonal antibody or replaced with lysozyme in a number of recent high resolution crystallographic analyses of GPCRs [23–26], since the inherent conformational flexibility of the loop poses a problem for x-ray crystallography. The lack of information from intracellular loops makes such crystallographic analyses somewhat limited. Another issue with many reported GPCR crystal structures is the fact that the receptor is crystallized in the lipidic cubic phase whose physiological significance is yet to be ascertained [27].

Although the number of reported crystal structures of GPCRs is continuously increasing [28], the challenge that remains is to generate a comprehensive understanding of the molecular mechanism underlying the conversion of ligand binding to GPCRs to receptor activation and signaling via a series of conformational changes. Keeping in mind this overall context, in this work, we have explored the organization and dynamics of the ICL3 of the serotonin_{1A} receptor. Human serotonin₁ receptors are classified into five subtypes 1A, 1B, 1D, 1E and 1F [8]. The serotonin_{1A} receptor is a prominent member of this subfamily. The receptor is estimated to have differentiated ~650 million years ago from the subfamily in the time period when vertebrates and invertebrates diverged, making this subtype an evolutionary marker [29, 30]. The intronless genomic clone for the human serotonin_{1A} receptor (G-21) encodes a protein of 422 amino acids [31]. The serotonin_{1A}

receptor is predominantly localized in the hippocampal region in the brain [32] and has not been purified from native tissue due to relatively low amounts present in it. As such, no crystal or NMR structure is available for this receptor, in spite of its importance as a drug target [8, 10]. We previously built a homology model for the receptor using the β_2 -adrenergic receptor template [33]. Due to the presence of three consensus sequences for N-linked glycosylation in the amino terminus, and ~48% homology of the receptor with β_2 -adrenergic receptor in the transmembrane region, it is predicted that the membrane topology of the receptor is such that its amino terminus faces the extracellular region and the carboxy terminus faces the intracellular cytoplasmic region [33] (see Fig. 1).

A striking aspect of the serotonin_{1A} receptor is the length (123 residues spanning from 221 to 343 residues, based on transmembrane helix prediction using TMHMM2 [15]) of its ICL3. This loop of the serotonin_{1A} receptor is considerably longer than the corresponding loop of other members of the serotonin₁ receptor subfamily [33, 34]. ICL3 has been shown to bind calmodulin [34, 35] and is important for coupling to G-proteins [36], crucial for downstream signaling. Sequence alignment of the members of the serotonin₁ receptor subfamily exhibits conserved sequences in the transmembrane regions, but not in the ICL3 region [33, 34]. This suggests that the diversity of function exhibited by various subtypes of serotonin₁ receptors could be encoded

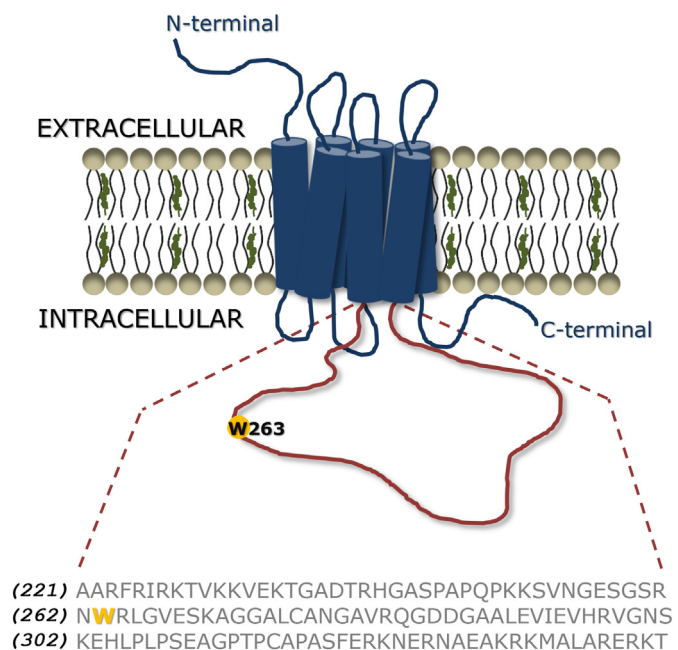


Fig. 1. A schematic representation of the topological features of the human serotonin_{1A} receptor highlighting the third intracellular loop (ICL3). The seven transmembrane helices embedded in the membrane bilayer (composed of phospholipids and cholesterol, typical constituents of eukaryotic membranes), and the receptor termini and loop regions connecting the transmembrane domains are shown. The transmembrane regions of the receptor have been predicted as putative α -helices using TMHMM2 [15]. The ICL3 segment (in maroon) with its amino acid sequence and its sole tryptophan residue (highlighted in yellow) are shown. ICL3 consists of 123 residues (residues 221–343) connecting transmembrane helices V and VI and is believed to play an important role in the recruitment of effectors (such as G-proteins) critical for downstream signaling, and binds calmodulin. See text for more details. (For interpretation of the references to colour in this figure legend, the reader is referred to the web version of this article.)

as sequence variations in the ICL3 region.

In this work, we expressed and purified the ICL3 region (see Fig. 1) of the serotonin_{1A} receptor in *E. coli* and monitored its motional restriction and organization utilizing the intrinsic fluorescence of the sole tryptophan and circular dichroism (CD) spectroscopy. Our results show constrained rotational dynamics of the tryptophan in ICL3, implying that the tryptophan residue is localized in a restricted microenvironment.

2. Materials and methods

2.1. Materials

β -mercaptoethanol, carbenicillin, chloramphenicol, dimethyl sulfoxide (DMSO), dithiothreitol (DTT), imidazole, isopropyl β -D-1-thiogalactopyranoside (IPTG), lysozyme, phenylmethylsulfonyl fluoride (PMSF), sodium phosphate, sodium chloride, streptomycin and urea (BioUltra grade) were obtained from Sigma Chemical Co. (St. Louis, MO). The HIS-MYC-HTR_{1A}-pDsRed-Monomer-Hyg-C1 vector was a generous gift from Dr. Mitradas M. Panicker, National Centre for Biological Sciences, Bangalore. Restriction enzymes were obtained from New England Biolabs (Ipswich, UK). Nonylphenyl polyethyleneglycol (NP-40) was obtained from Calbiochem (San Diego, CA). 2-(4-(2-Hydroxyethyl)piperazin-1-yl)ethanesulfonic acid (HEPES) was purchased from Affymetrix (Santa Clara, CA). The concentration of ICL3 was estimated from its molar extinction coefficient of $5500 \text{ M}^{-1} \text{ cm}^{-1}$ at 280 nm, as predicted using the ProtParam tool in ExPASy [37]. All other chemicals and solvents used were of the highest available purity. Water was purified through a Millipore (Bedford, MA) Milli-Q system and used throughout.

2.2. Methods

2.2.1. ICL3 cloning, expression and purification

The HIS-MYC-HTR_{1A}-pDsRed-Monomer-Hyg-C1 vector was double digested with restriction enzymes, NheI and AgeI, to obtain a gene containing the coding region of the serotonin_{1A} receptor DNA. ICL3 (amino acid region: 221–343 of the human serotonin_{1A} receptor, see Fig. 1) was PCR amplified and double digested with restriction enzymes, NdeI and BamHI, and ligated into pET16b vector using standard molecular biology techniques. The plasmid codes for a decahistidine tag

followed by a Factor Xa cleavage site at the N-terminus of ICL3 with an engineered stop codon post the ICL3 gene. The pET16b-ICL3 plasmid containing ICL3 and additional features were confirmed using standard gene sequencing methods.

The pET16b-ICL3 plasmid was transformed into *E. coli* BL21-CodonPlus (DE3)-RIPL competent cells and cells were grown on LB plates containing 34 $\mu\text{g}/\text{ml}$ of chloramphenicol, 50 $\mu\text{g}/\text{ml}$ of carbenicillin and 100 $\mu\text{g}/\text{ml}$ of streptomycin. Single bacterial colony was picked from the transformation plate, transferred to 10 ml of LB medium with the above antibiotics and incubated overnight at 37 °C, 200 rpm. The culture was transferred into 1 l LB medium containing the above antibiotics and incubated at 37 °C, 200 rpm. The culture was induced when OD₆₀₀ reached 0.8 using 1 mM of IPTG and further incubated for 3.5 h, 240 rpm at 25 °C. Cells were harvested by centrifugation at $6200 \times g$ for 8 min at 4 °C.

The cell pellet was suspended in a lysis buffer containing 20 mM HEPES/500 mM NaCl/10 mM imidazole (pH 7.5), 10 mM β -mercaptoethanol, 0.5% NP-40 and 1 mM PMSF and incubated on ice with 1 mg/ml of lysozyme for 30 min. After incubation, cells were broken by sonication on ice and cell lysates containing the cytosolic fraction was separated by centrifugation at $26,850 \times g$ for 40 min at 4 °C. The supernatant was mixed with Ni²⁺-NTA resin (Qiagen, Hilden, Germany) in a glass column by nutating at 4 °C for 45 min. The resin loaded with ICL3 was washed with seven resin volumes of washing buffer containing 20 mM HEPES/500 mM NaCl/30 mM imidazole (pH 7.5) and 10 mM β -mercaptoethanol to remove nonspecific protein binding to the resin. The pure fractions of ICL3 were eluted with wash buffer containing increasing concentration of imidazole (50–250 mM).

The eluted fractions of ICL3 were pooled and subjected to a high level of purification (> 95%) using size exclusion chromatography with a preparative Superdex G75 gel filtration column (GE Life Sciences, Marlborough, MA). The column was pre-equilibrated with two column volumes of purification buffer containing 10 mM sodium phosphate/150 mM NaCl (pH 7.0) and 1 mM DTT. The recombinant ICL3 eluted at the corresponding volume of a ~ 16 kDa protein, as evident from the gel filtration profile and SDS-PAGE analysis (see Fig. 2). The purified peptide was lyophilized and stored at -30 °C.

2.2.2. Sample preparation

Fresh ICL3 samples were prepared for each experiment by dissolving the lyophilized peptide in Milli-Q water and diluting with 10 mM

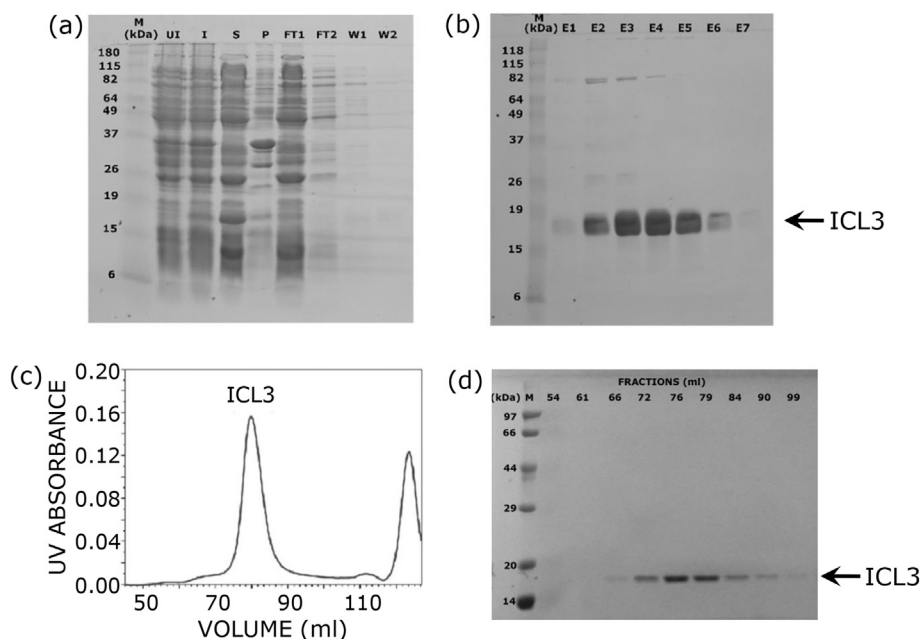


Fig. 2. Purification of ICL3. (a) Ni²⁺-NTA purification of ICL3 analyzed by SDS-PAGE; M: molecular weight marker, UI: uninduced fraction, I: induced fraction, S: supernatant, P: pellet, FT1: 1st flow through, FT2: 2nd flow through, W1 and W2: washes with 30 mM imidazole. (b) Elution fractions of Ni²⁺-NTA purification on SDS PAGE; E1-E5: elutions with wash buffer containing increasing concentration of imidazole (50–250 mM, 50 mM gradient step), E6 and E7: wash buffer with 250 mM imidazole. The ICL3 band is marked with an arrow. (c) Size exclusion chromatogram of the pooled elution fraction E2-E6 from (b) using a preparative Superdex G75 column. An isolated peak containing pure fractions of ICL3 is shown. (d) SDS-PAGE analysis of samples collected in (c). M: molecular weight marker, the loaded fractions (in ml) and band corresponding to ICL3 (~ 16 kDa) are marked. See Materials and methods for more details.

sodium phosphate/150 mM NaCl (pH 7.0) buffer. The final peptide concentration was 20 μ M for both fluorescence and circular dichroism spectroscopic measurements. ICL3 was denatured by incubation with 8 M urea for 2 h prior to data acquisition. The concentration of urea in water was estimated with a Brixus CRI375P-01U refractometer (Sartorius AG, Goettingen, Germany) according to the following equation [38]:

$$C = 117.66(\Delta N) + 29.753(\Delta N)^2 + 185.56(\Delta N)^3 \quad (1)$$

where C is the concentration of urea in molarity and ΔN is the change in refractive index of the urea solution relative to that of water.

2.2.3. Steady state fluorescence measurements

Steady state fluorescence measurements were performed with a Hitachi F-7000 spectrofluorometer (Tokyo, Japan) using 1 cm path length quartz cuvette. Excitation and emission slits with slit widths of 2.5 and 5 nm, respectively, were used for all measurements. All spectra were recorded in the corrected spectrum mode. Background intensities of samples in which the peptide was omitted were negligible in most cases and were subtracted from each sample spectrum to cancel out any contribution due to the solvent Raman peak and other scattering artifacts. Data shown are representative of at least four independent measurements and the observed emission maxima were identical or within ± 1 nm of the values reported.

Fluorescence anisotropy measurements were performed at room temperature ($\sim 25^\circ\text{C}$) with a Hitachi polarization accessory. Fluorescence anisotropy values were calculated using the following equation [39]:

$$r = \frac{I_{VV} - GI_{VH}}{I_{VV} + 2GI_{VH}} \quad (2)$$

where I_{VV} and I_{VH} are the measured fluorescence intensities (after appropriate background subtraction) with the excitation polarizer vertically oriented and emission polarizer vertically and horizontally oriented, respectively. G is the grating correction factor and is the ratio of the efficiencies of the detection system for vertically and horizontally polarized light, and is equal to I_{HV}/I_{HH} . Excitation and emission slits with slit widths of 2.5 and 5 nm, respectively, were used for all measurements. Data shown are means \pm S.E. of at least four independent measurements.

2.2.4. Time-resolved fluorescence measurements

Fluorescence lifetimes were calculated from time-resolved fluorescence intensity decays using Delta-D TCSPC system (Horiba Jobin Yvon IBH, Glasgow, UK) with EzTime software version 3.2.2.4 (Horiba Scientific, Edison, NJ) in the time-correlated single photon counting (TCSPC) mode. A pulsed light-emitting diode (DD-290) was used as an excitation source. This LED generates optical pulses at 297 nm with a typical pulse width of 0.8 ns and is run at a 20 MHz repetition rate. The instrument response function (IRF) (also known as the LED profile) was measured at the excitation wavelength with Ludox (colloidal silica) as a scatterer. In order to optimize the signal-to-noise ratio, 10,000 photon counts were collected at the peak channel. Data acquisition was carried out using emission slit widths of 8 nm or less and with a neutral density filter (ND1) in the excitation path. The sample and the scatterer profiles were acquired in 10 alternate cycles of 1,000 photon counts (10% acquisition) at each of the peak channels, to compensate for shape and timing drifts occurring in the course of data acquisition. This arrangement has the additional advantage of preventing prolonged exposure and subsequent photodamage of the fluorophore.

Data were stored and analyzed using the in-built plugins in the EzTime software version 3.2.2.4 (Horiba Scientific, Edison, NJ). Fluorescence intensity decay curves were deconvoluted with the IRF and analyzed as a sum of exponential terms given by the equation:

$$F(t) = \sum_i \alpha_i \exp(-t/\tau_i) \quad (3)$$

where $F(t)$ is the fluorescence intensity at time t and α_i is a pre-exponential factor denoting the fractional contribution to the time-resolved decay of the i^{th} component with a lifetime of τ_i , such that $\sum_i \alpha_i = 1$. The decay parameters were recovered using a nonlinear least squares iterative fitting program based on the Marquadt algorithm [40]. The program also includes subroutine packages associated with statistical analysis and plotting [41]. The goodness of fit of a given data set to a chosen function was evaluated by the χ^2 ratio, the weighted residuals [42] and the autocorrelation function of the weighted residuals [43]. A fit was considered acceptable when plots of the weighted residuals and their autocorrelation function exhibited random deviation about zero, with a χ^2 value of not more than 1.1. Intensity-averaged mean fluorescence lifetimes ($\langle \tau \rangle$) for triexponential fluorescence decays were calculated from the decay times and pre-exponential factor using the equation [39]:

$$\langle \tau \rangle = \frac{\alpha_1 \tau_1^2 + \alpha_2 \tau_2^2 + \alpha_3 \tau_3^2}{\alpha_1 \tau_1 + \alpha_2 \tau_2 + \alpha_3 \tau_3} \quad (4)$$

2.2.5. CD measurements and deconvolution

CD measurements were carried out at room temperature ($\sim 25^\circ\text{C}$) with a JASCO J-815 spectropolarimeter (Tokyo, Japan) calibrated with (+)-10-camphorsulfonic acid [44]. Spectra were scanned in a quartz optical sandwich cell with a path length of 0.01 cm, and recorded in 0.5 nm wavelength increments with a band width of 2 nm and a response time of 1 s. For monitoring changes in secondary structure, spectra were scanned from 190 to 260 nm in the far-UV range. The scan rate was 50 nm/min and each spectrum is the average of 10 continuous scans with a full scale sensitivity of 100 mdeg. Spectra were corrected for background by subtraction of appropriate blanks. Data are represented as mean residue ellipticities and calculated using the equation:

$$[\theta] = \theta_{\text{obs}}/(10Cl) \quad (5)$$

where θ_{obs} is the observed ellipticity in mdeg, l is the path length in cm, and C is the concentration of peptide bonds in mol/l.

The far-UV CD spectra of ICL3 in buffer was deconvoluted with the web-based CD analysis resource, DichroWeb [45, 46], using the CDSSTR analysis method [47] with SMP180 [48] as the reference data set. In addition, for the purpose of representation, the CD spectra were subjected to a moderate degree of smoothening by the adjacent averaging program available in Microcal Origin version 8.0 (OriginLab, Northampton, MA), while ensuring that the overall spectral shape remains unaltered.

2.2.6. Data analysis and plotting

Student's two-tailed unpaired t -test was performed to estimate significance levels using Graphpad Prism software, version 4.0 (San Diego, CA). Data plots were generated with Microcal Origin version 8.0 (OriginLab, Northampton, MA).

3. Results

3.1. ICL3 purification and characterization

The cloning, heterologous expression and purification of ICL3 (corresponding to amino acids 221–343 of the human serotonin_{1A} receptor, see Fig. 1) was carried out in *E. coli* as described in Materials and methods (Fig. 2). The recombinant ICL3 eluted as a ~ 16 kDa protein in the gel filtration column and in SDS-PAGE analysis (see Fig. 2c,d).

3.2. Wavelength-selective fluorescence of the sole tryptophan in ICL3: REES and related effects

Red Edge Excitation Shift (REES) is a phenomenon often observed in case of fluorophores localized in a motionally restricted environment,

such as at the membrane interface or in dynamically constrained regions of proteins [49–51]. A major factor governing REES is that the fluorophore should experience an environment in which the rate of solvent relaxation in the excited state is slow relative to fluorescence lifetime. REES is expressed as the shift in the wavelength of maximum fluorescence emission toward higher wavelengths, induced by a shift in the excitation wavelength toward the red edge of absorption spectrum. The shift in the wavelength of maximum fluorescence emission of the sole tryptophan (residue 263) of ICL3 (see Fig. 1) in buffer as a function of excitation wavelength is shown in Fig. 3a (the inset displays tryptophan emission spectra at representative excitation wavelengths). The figure shows that there is a shift in the emission maximum from 345 to 349 nm, corresponding to REES of 4 nm, in response to change in excitation wavelength from 280 to 307 nm. This indicates that the sole tryptophan residue of ICL3 experiences motionally restricted environment.

Fluorophores exhibiting REES often show wavelength-dependence of fluorescence anisotropy [49,52]. The excitation anisotropy spectra (i.e., a plot of fluorescence anisotropy vs. excitation wavelength) of ICL3 in buffer is shown in Fig. 3b. The figure shows that the anisotropy of ICL3 tryptophan displays substantial change (~110%) upon increasing the excitation wavelength from 280 to 305 nm, with a steep increase toward the red edge. This type of excitation wavelength dependent change in fluorescence anisotropy is typical for fluorophores in restricted environment [53]. This increase in fluorescence anisotropy with increasing excitation wavelength could be because of decreased rotational rate of the fluorophore in the solvent-relaxed state (the subpopulation that is photoselected upon red edge excitation) because of strong dipolar interactions with the surrounding solvent molecules [52]. It should be noted here that Fig. 3b shows an initial dip in fluorescence anisotropy at ~290 nm. This is typical of tryptophan in restricted environment [54] and has to do with complex photophysics of the two overlapping, mutually orthogonal S_0-S_1 electronic transitions (1L_a and 1L_b) of tryptophan (for details, see [50,54]).

REES arises due to photoselection of a subpopulation of excited state fluorophores upon excitation at longer wavelengths, giving rise to differential extents of solvent reorientation corresponding to each excitation wavelength. Since fluorescence lifetime is known to be sensitive to local environment [55], differential extents of solvent relaxation around a fluorophore gives rise to different lifetimes. Fig. 4a shows the effect of increasing emission wavelength on the mean fluorescence lifetime of the ICL3 tryptophan. The intensity-averaged mean fluorescence lifetimes at different emission wavelengths were calculated using Eq. (4) and are shown in Table 1. The mean fluorescence lifetime is independent of the method of analysis and the number of exponentials used to fit the time-resolved fluorescence decay. A representative decay profile of ICL3 in buffer with its triexponential fitting and the associated statistical parameters used to check the goodness of fit are shown in Fig. S1. Fig. 4a shows that the mean fluorescence lifetime exhibits a considerable increase (~27%) with increasing emission wavelength across the emission spectrum (320–380 nm). Emission at shorter wavelengths originates predominantly from solvent unrelaxed fluorophores, characterized by shorter fluorescence lifetimes. This is because this subpopulation would decay both at the rate of fluorescence emission at the given excitation wavelength and by decay to longer wavelengths (which remain unobserved due to the choice of emission wavelength). On the other hand, fluorophore populations selected at the longer emission wavelength (red edge) are more relaxed due to an appreciably higher time spent in the excited state (i.e., longer lifetime).

Fig. 4b shows the reduction in fluorescence anisotropy (~43%) with increasing emission wavelength. As discussed, longer emission wavelengths photoselect longer-lived fluorophores, which have more time to rotate in the excited state. This leads to greater extent of depolarization and lower values of fluorescence anisotropy at the red edge.

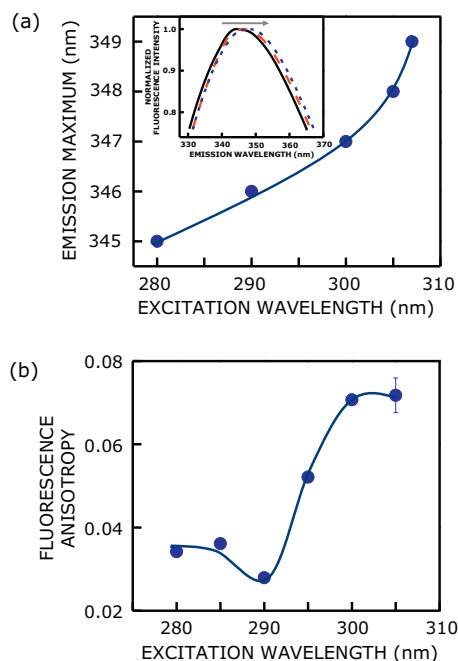


Fig. 3. Wavelength-selective fluorescence of ICL3: change in fluorescence emission parameters with excitation wavelength. (a) Increase in the wavelength of maximum emission with increasing excitation wavelength, corresponding to REES of 4 nm. Data shown are representative of at least four independent measurements and the observed emission maxima were identical or within ± 1 nm of the values reported. The inset shows the progressive shift in the tryptophan emission maximum upon excitation at 280 nm (—); 300 nm (---); and 305 nm (····). Spectra shown are intensity-normalized at the respective emission maximum. (b) Change in fluorescence anisotropy with increasing excitation wavelength. Emission wavelength was 345 nm. Data represent means \pm S.E. of at least four independent measurements. Lines joining the data points are provided merely as viewing guides. The concentration of ICL3 was 20 μ M. See Materials and methods for other details.

3.3. Effect of denaturation on REES and rotational dynamics

The above results imply that the sole tryptophan in ICL3 is in a microenvironment that induces constrained dynamics in the fluorophore. Such motional restriction is known to be associated with soluble proteins characterized by well-defined secondary structural elements [53]. In the case of ICL3, the motional restriction of the tryptophan could be due to the constraints induced by the peptide secondary structure. To further explore this, we monitored the change in maximum of fluorescence emission with excitation wavelength for denatured ICL3 (see Fig. 5a). The figure shows complete lack of REES in denatured ICL3, since there was no shift in the emission maximum even when excitation wavelength was changed from 280 to 307 nm, although there was a shift in the emission maximum itself (from 345 to 348 nm). The red shift (3 nm) in the emission maximum could be due to greater exposure to polar bulk water upon denaturation.

To confirm the contribution of the peptide secondary structure in inducing motional restriction of the sole tryptophan in ICL3, we carried out CD spectroscopic measurements. Fig. 5b shows the far-UV CD spectra of ICL3 in buffer and upon denaturation. The CD spectrum of ICL3 in buffer showed some contribution from α -helical elements. Spectral deconvolution of the CD spectrum of ICL3 in buffer with Dichroweb [43, 44] indicated that the peptide consists of ~18% α -helix, 18% β -sheet, 17% turn and 47% random coil, in overall agreement with previous reports [34,56]. The CD spectrum of the denatured ICL3, however, showed lack of secondary structural elements. These results are in agreement with our results (Fig. 5a), in which REES was observed only in case of ICL3 in buffer, but not upon denaturation.

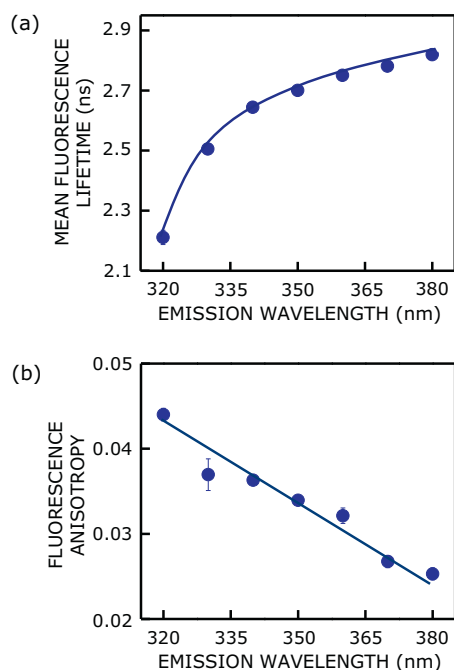


Fig. 4. Emission wavelength-dependent fluorescence of ICL3: change in fluorescence anisotropy and lifetime with emission wavelength. (a) Effect of increasing emission wavelength on the mean intensity-averaged fluorescence lifetime of ICL3. The excitation wavelength was 297 nm. Mean fluorescence lifetimes were calculated from Table 1 using Eq. (4). (b) Reduction in fluorescence anisotropy with increasing emission wavelength. Excitation wavelength was kept constant at 280 nm. Lines joining the data points are provided merely as viewing guides. Data represent means \pm S.E. of at least four independent measurements. The concentration of ICL3 was 20 μ M. All other conditions are as in Fig. 3. See Materials and methods for more details.

Table 1
Representative fluorescence lifetimes of native and denatured ICL3^a.

Emission wavelength (nm)	α_1	τ_1 (ns)	α_2	τ_2 (ns)	α_3	τ_3 (ns)	$\langle \tau \rangle^b$ (ns)	χ^2
(a) ICL3 in buffer								
320	0.21	1.44	0.09	3.68	0.70	0.19	2.19	1.1
330	0.40	1.83	0.15	4.05	0.45	0.43	2.53	1.1
340	0.45	1.93	0.17	4.10	0.38	0.53	2.63	1.1
345 ^c	0.46	1.96	0.18	4.12	0.36	0.56	2.68	1.1
350	0.48	2.07	0.16	4.28	0.36	0.62	2.70	1.1
360	0.49	2.13	0.16	4.33	0.35	0.63	2.74	1.1
370	0.51	2.17	0.16	4.37	0.33	0.65	2.77	1.1
380	0.53	2.21	0.15	4.48	0.32	0.65	2.79	1.1
(b) Denatured ICL3								
348 ^c	0.42	2.28	0.30	4.62	0.28	0.49	3.49	1.1

^a Excitation wavelength was 297 nm. The number of photons collected at the peak channel was 10,000. The concentration of ICL3 was 20 μ M. All other conditions are as in Fig. 4a. See Materials and methods for other details.

^b Calculated using Eq. (4).

^c At the respective emission maximum.

Fluorescence anisotropy of ICL3 in buffer and upon denaturation is shown in Fig. 6a. The anisotropy of ICL3 in buffer (0.034) was found to be higher than that of denatured ICL3 (0.026), thereby indicating that the environment around the tryptophan residue in ICL3 in buffer is more restrictive. To ensure that the reported anisotropy values are not influenced by lifetime-induced artifacts, the apparent (average) rotational correlation times were calculated using Perrin's equation [39]:

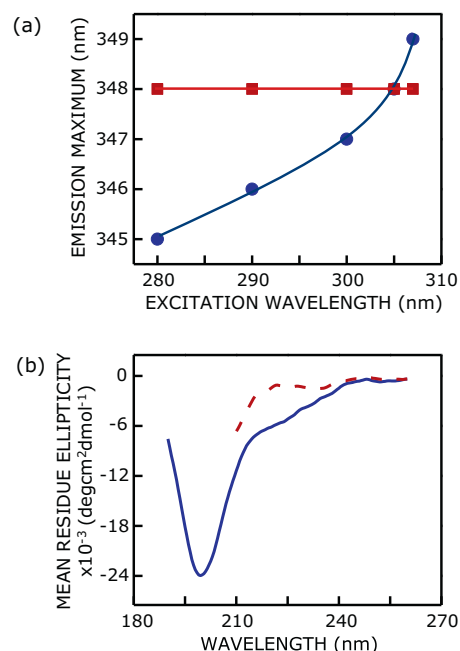


Fig. 5. Effect of denaturation on tryptophan REES and secondary structure of ICL3. (a) The absence of any shift in wavelength of maximum emission with increasing excitation wavelength upon denaturation (■). REES of ICL3 in buffer (●) is shown as a control (from Fig. 3a). Denaturation was carried out with 8 M urea. Data shown are representative of at least four independent measurements and the observed emission maxima were identical or within ± 1 nm of the values reported. Lines joining the data points are provided merely as viewing guides. (b) Representative far-UV CD spectra of ICL3 in buffer (—) and denatured (---) conditions. CD data below 210 nm were not recorded in case of denatured ICL3 due to high absorbance of urea at lower wavelengths. The concentration of ICL3 was 20 μ M in all cases. All other conditions are as in Fig. 3. See Materials and methods for more details.

$$\tau_c = \frac{\langle \tau \rangle r}{r_0 - r} \quad (6)$$

where r_0 is the fundamental anisotropy of tryptophan, r is the steady state anisotropy taken from Fig. 6a, and $\langle \tau \rangle$ is the mean fluorescence lifetime (from Table 1). The value of r_0 was taken to be 0.16 [57]. Fig. 6b shows that the apparent rotational correlation time of the ICL3 tryptophan in buffer (0.72 ns) was significantly higher than of the denatured peptide (0.65 ns), thereby validating the anisotropy trend. However, since the presence of 8 M urea in denatured ICL3 would increase the bulk viscosity, the rotational correlation time reported for the denatured ICL3 is an upper estimate and the actual difference in rotational correlation time could be more.

4. Discussion

A recent trend in GPCR structure-function analysis has been to explore regions of GPCRs that are structured and disordered [58]. It appears that the diversity and synthesis of structured and disordered regions in GPCRs are crucial in generating the diverse functions of GPCRs. While the structured transmembrane domains continue to be the major focus, the disordered regions of GPCRs are yet to be appreciated for their role in GPCR function. The molecular architecture and topology of GPCRs in general, and the serotonin_{1A} receptor in particular, suggests that the conversion of ligand-induced subtle transmembrane conformational rearrangements into downstream signaling pathways is mediated by extramembranous regions such as ICL3. Previous reports have highlighted the crucial role of ICL3 in receptor activation *via* interaction with downstream effectors such as G-proteins and β -arrestin [9, 16–22]. Disordered regions in GPCRs are believed to increase the

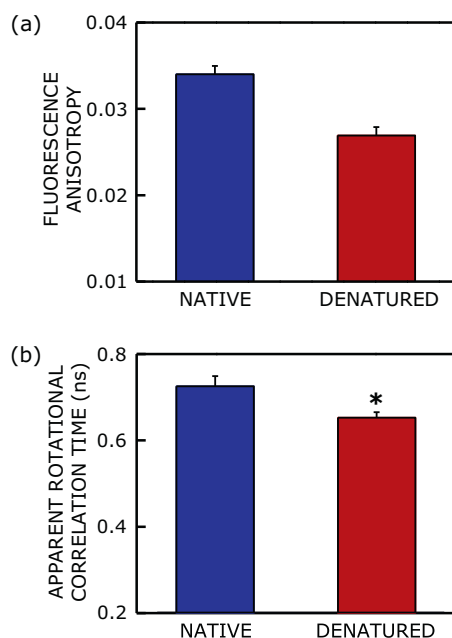


Fig. 6. Effect of denaturation on rotational dynamics of ICL3. (a) Fluorescence anisotropy of ICL3 in buffer and upon denaturation. The excitation wavelength was 280 nm and emission was monitored at the respective emission maximum, i.e., at 345 (buffer) and 348 (denatured) nm. (b) Apparent rotational correlation times of ICL3 in buffer and upon denaturation. Apparent rotational correlation times were calculated from fluorescence anisotropy and mean fluorescence lifetime (from Fig. 6a and Table 1, respectively) using Eq. (6). Data represent means \pm S.E. of at least four independent measurements (* corresponds to significant ($p < 0.05$) difference in apparent rotational correlation time of denatured ICL3 relative to ICL3 in buffer). See Materials and methods, and Results sections for more details.

functional repertoire of GPCRs *via* conformational plasticity [58,59]. The third intracellular loop in GPCRs is considered to be intrinsically disordered and the length of the loop varies among different GPCRs. In case of the serotonin_{1A} receptor, the third intracellular loop has been shown to be crucial in coupling to and activation of G-proteins [56,60]. Interestingly, it has been previously reported using site-directed mutagenesis that mutations in ICL3 of the serotonin_{1A} receptor alters G-protein coupling from G_i to G_s in a ligand-dependent manner [36].

In this work, we show that the sole tryptophan in the peptide corresponding to the ICL3 region of the serotonin_{1A} receptor exhibits REES of 4 nm, thereby implying motional restriction of the tryptophan due to the constraints induced by the peptide secondary structure. These results are supported by wavelength-dependent changes in fluorescence anisotropy and lifetime. The motional restriction was relaxed upon denaturation of the peptide, suggesting the involvement of the peptide secondary structure in it. These results are further supported by CD spectroscopy and apparent rotational correlation time measurement. These novel results constitute one of the first observations of motional restriction in the ICL3 region in GPCRs, and assume relevance in the overall context of the largely unexplored role of loop regions in GPCR organization and function.

We should note here that the restricted dynamics of the ICL3 tryptophan reported here could be a lower limit of the natural constraint experienced by the tryptophan in the untruncated receptor since ICL3 would be linked to the rest of the receptor in such a case. We previously reported that REES is a sensitive and convenient approach to explore the dynamic organization of proteins in all states (native, intrinsically disordered (molten globule), amyloid and denatured) [50,61]. Previous work from our laboratory has established the importance of tryptophan residues and their characteristic environment-dependent constrained dynamics in the context of structure and function of proteins and

peptides [61–65]. Our observation of REES in ICL3 tryptophan assumes relevance in this context and is reinforced by an earlier report on the involvement of the sole tryptophan residue in the binding of calmodulin to ICL3 [34]. This report, along with our observation of a complete loss of tryptophan constrained dynamics upon urea denaturation of the peptide, indicates that the secondary structural elements responsible for calmodulin binding are possibly involved in imposing the restriction on tryptophan rotational dynamics. We envision that analysis of structure and dynamics of the extramembraneous regions of GPCRs, in combination with knowledge gained from transmembrane domains, would provide a comprehensive understanding of GPCR function in health and disease.

Acknowledgments

This work was supported by the Science and Engineering Research Board (Govt. of India) project (EMR/2016/002294) to A.C. and by the Council of Scientific and Industrial Research, Govt. of India, Network project GenCODE (BSC0123) to M.V.D. A.C. gratefully acknowledges support from J.C. Bose Fellowship (Department of Science and Technology, Govt. of India). S.P. and P.S. thank the University Grants Commission and the Council of Scientific and Industrial Research, Govt. of India, for the awards of Senior Research Fellowship and Shyama Prasad Mukherjee Fellowship, respectively. A.C. is an Adjunct Professor of Tata Institute of Fundamental Research (Mumbai), RMIT University (Melbourne, Australia), Indian Institute of Technology (Kanpur), and Indian Institute of Science Education and Research (Mohali). We gratefully acknowledge Dr. Mitradas M. Panicker (National Centre for Biological Sciences, Bangalore) for the generous gift of the HIS-MYC-HTR_{1A}-pDsRed-Monomer-Hyg-C1 plasmid. We thank Dr. B. Raman for technical help and members of the Chattopadhyay laboratory for their comments and discussions.

Declarations of interest

None.

Appendix A. Supplementary data

Supplementary data to this article can be found online at <https://doi.org/10.1016/j.bpc.2018.05.008>.

References

- [1] K.L. Pierce, R.T. Premont, R.J. Lefkowitz, Seven-transmembrane receptors, *Nat. Rev. Mol. Cell Biol.* 3 (2002) 639–650.
- [2] D.M. Rosenbaum, S.G.F. Rasmussen, B.K. Kobilka, The structure and function of G-protein-coupled receptors, *Nature* 459 (2009) 356–363.
- [3] A. Chattopadhyay, GPCRs: lipid-dependent membrane receptors that act as drug targets, *Adv. Biol.* 2014 (2014) 143023.
- [4] K.A. Jacobson, New paradigms in GPCR drug discovery, *Biochem. Pharmacol.* 98 (2015) 541–555.
- [5] R.M. Cooke, A.J.H. Brown, F.H. Marshall, J.S. Mason, Structures of G protein-coupled receptors reveal new opportunities for drug discovery, *Drug Discov. Today* 20 (2015) 1355–1364.
- [6] A. Chattopadhyay (Ed.), *Serotonin Receptors in Neurobiology*, CRC Press, Boca Raton, FL, 2007.
- [7] D.E. Nichols, C.D. Nichols, Serotonin receptors, *Chem. Rev.* 108 (2008) 1614–1641.
- [8] F. Fiorino, B. Severino, E. Magli, A. Ciano, G. Caliendo, V. Santagada, F. Frecentese, E. Perissutti, 5-HT_{1A} receptor: an old target as a new attractive tool in drug discovery from central nervous system to cancer, *J. Med. Chem.* 57 (2014) 4407–4426.
- [9] T.J. Pucadyil, S. Kalipatnapu, A. Chattopadhyay, The serotonin_{1A} receptor: a representative member of the serotonin receptor family, *Cell. Mol. Neurobiol.* 25 (2005) 553–580.
- [10] E. Lacivita, M. Leopoldo, F. Berardi, R. Perrone, 5-HT_{1A} receptor, an old target for new therapeutic agents, *Curr. Top. Med. Chem.* 8 (2008) 1024–1034.
- [11] T.J. Pucadyil, A. Chattopadhyay, Role of cholesterol in the function and organization of G-protein coupled receptors, *Prog. Lipid Res.* 45 (2006) 295–333.
- [12] Y.D. Paila, A. Chattopadhyay, Membrane cholesterol in the function and organization of G-protein coupled receptors, *Subcell. Biochem.* 51 (2010) 439–466.
- [13] M. Jafurulla, A. Chattopadhyay, Membrane lipids in the function of serotonin and adrenergic receptors, *Curr. Med. Chem.* 20 (2013) 47–55.

- [14] M. Jafurulla, A. Chattopadhyay, Sphingolipids in the function of G protein-coupled receptors, *Eur. J. Pharmacol.* 763 (2015) 241–246.
- [15] A. Krogh, B. Larsson, G. von Heijne, E.L.L. Sonnhammer, Predicting transmembrane protein topology with a hidden Markov model: application to complete genomes, *J. Mol. Biol.* 305 (2001) 567–580.
- [16] E.R. Prossnitz, O. Quehenberger, C.G. Cochrane, R.D. Ye, The role of the third intracellular loop of the neutrophil N-formyl peptide receptor in G protein coupling, *Biochem. J.* 294 (1993) 581–587.
- [17] P. Wonerow, T. Schöneberg, G. Schultz, T. Gudermann, R. Paschke, Deletions in the third intracellular loop of the thyrotropin receptor. A new mechanism for constitutive activation, *J. Biol. Chem.* 273 (1998) 7900–7905.
- [18] J.L. DeGraff, V.V. Gurevich, J.L. Benovic, The third intracellular loop of α_2 -adrenergic receptors determines subtype specificity of arrestin interaction, *J. Biol. Chem.* 277 (2002) 43247–43252.
- [19] K. Chakir, Y. Xiang, D. Yang, S.-J. Zhang, H. Cheng, B.K. Kobilka, R.-P. Xiao, The third intracellular loop and the carboxyl terminus of β_2 -adrenergic receptor confer spontaneous activity of the receptor, *Mol. Pharmacol.* 64 (2003) 1048–1058.
- [20] S.P. Pydi, N. Singh, J. Upadhyaya, R.P. Bhullar, P. Cheikani, The third intracellular loop plays a critical role in bitter taste receptor activation, *Biochim. Biophys. Acta* 1838 (2014) 231–236.
- [21] O. Ozcan, A. Uyar, P. Doruker, E.D. Akten, Effect of intracellular loop 3 on intrinsic dynamics of human β_2 -adrenergic receptor, *BMC Struct. Biol.* 13 (2013) 29.
- [22] J. Huang, S.K. Lakkaraju, A. Coop, A.D. MacKerell Jr., Conformational heterogeneity of intracellular loop 3 of the μ -opioid G-protein coupled receptor, *J. Phys. Chem. B* 120 (2016) 11897–11904.
- [23] P.W. Day, S.G.F. Rasmussen, C. Parnot, J.J. Fung, A. Masood, T.S. Kobilka, X.-J. Yao, H.-J. Choi, W.I. Weis, D.K. Rohrer, B.K. Kobilka, A monoclonal antibody for G protein-coupled receptor crystallography, *Nat. Methods* 4 (2007) 927–929.
- [24] V. Cherezov, D.M. Rosenbaum, M.A. Hanson, S.G.F. Rasmussen, F.S. Thian, T.S. Kobilka, H.-J. Choi, P. Kuhn, W.I. Weis, B.K. Kobilka, R.C. Stevens, High-resolution crystal structure of an engineered human β_2 -adrenergic G protein-coupled receptor, *Science* 318 (2007) 1258–1265.
- [25] D.M. Rosenbaum, V. Cherezov, M.A. Hanson, S.G.F. Rasmussen, F.S. Thian, T.S. Kobilka, H.-J. Choi, X.-J. Yao, W.I. Weis, R.C. Stevens, B.K. Kobilka, GPCR engineering yields high-resolution structural insights into β_2 -adrenergic receptor function, *Science* 318 (2007) 1266–1273.
- [26] E. Ghosh, P. Kumari, D. Jainan, A.K. Shukla, Methodological advances: the unsung heroes of the GPCR structural revolution, *Nat. Rev. Mol. Cell Biol.* 16 (2015) 69–81.
- [27] G. Khelashvili, P.B.C. Albornoz, N. Johner, S. Mondal, M. Caffrey, H. Weinstein, Why GPCRs behave differently in cubic and lamellar lipidic mesophases, *J. Am. Chem. Soc.* 134 (2012) 15858–15868.
- [28] E. Ghosh, K. Nidhi, A.K. Shukla, SnapShot: GPCR-ligand interactions, *Cell* 159 (2014) 1712–1712.e1.
- [29] S.J. Peroutka, T.A. Howell, The molecular evolution of G protein-coupled receptors: focus on 5-hydroxytryptamine receptors, *Neuropharmacology* 33 (1994) 319–324.
- [30] T. Schöneberg, M. Hofreiter, A. Schulz, H. Römpler, Learning from the past: evolution of GPCR functions, *Trends Pharmacol. Sci.* 28 (2007) 117–121.
- [31] A. Fargin, J.R. Raymond, M.J. Lohse, B.K. Kobilka, M.G. Caron, R.J. Lefkowitz, The genomic clone G-21 which resembles a β -adrenergic receptor sequence encodes the 5-HT_{1A} receptor, *Nature* 335 (1988) 358–360.
- [32] J.M. Palacios, C. Waeber, D. Hoyer, G. Mengod, Distribution of serotonin receptors, *Ann. N. Y. Acad. Sci.* 600 (1990) 36–52.
- [33] Y.D. Paila, S. Tiwari, D. Sengupta, A. Chattopadhyay, Molecular modeling of the human serotonin_{1A} receptor: role of membrane cholesterol in ligand binding of the receptor, *Mol. Biosyst.* 7 (2011) 224–234.
- [34] A.S. Chen, Y.M. Kim, S. Gayen, Q. Huang, M. Raida, C. Kang, NMR structural study of the intracellular loop 3 of the serotonin 5-HT_{1A} receptor and its interaction with calmodulin, *Biochim. Biophys. Acta* 1808 (2011) 2224–2232.
- [35] J.H. Turner, A.K. Gelasco, J.R. Raymond, Calmodulin interacts with the third intracellular loop of the serotonin 5-hydroxytryptamine_{1A} receptor at two distinct sites. Putative role in receptor phosphorylation by protein kinase C, *J. Biol. Chem.* 279 (2004) 17027–17037.
- [36] A. Malmberg, P.G. Strange, Site-directed mutations in the third intracellular loop of the serotonin 5-HT_{1A} receptor alter G protein coupling from G_i to G_s in a ligand-dependent manner, *J. Neurochem.* 75 (2000) 1283–1293.
- [37] E. Gasteiger, C. Hoogland, A. Gattiker, S. Duvaud, M.R. Wilkins, R.D. Appel, A. Bairoch, Protein identification and analysis tools on the ExPASy server, in: J.M. Walker (Ed.), *The Proteomics Protocols Handbook*, Humana Press, Totowa, NJ, 2005, pp. 571–607.
- [38] C.N. Pace, Determination and analysis of urea and guanidine hydrochloride denaturation curves, *Methods Enzymol.* 131 (1986) 266–280.
- [39] J.R. Lakowicz, *Principles of Fluorescence Spectroscopy*, third ed., Springer, New York, 2006.
- [40] P.R. Bevington, *Data Reduction and Error Analysis for the Physical Sciences*, McGraw-Hill, New York, 1969.
- [41] D.V. O'Connor, D. Phillips, *Time-correlated Single Photon Counting*, Academic Press, London, 1984, pp. 180–189.
- [42] R.A. Lampert, L.A. Chewter, D. Phillips, D.V. O'Connor, A.J. Roberts, S.R. Meech, Standards for nanosecond fluorescence decay time measurements, *Anal. Chem.* 55 (1983) 68–73.
- [43] A. Grinvald, I.Z. Steinberg, On the analysis of fluorescence decay kinetics by the method of least-squares, *Anal. Biochem.* 59 (1974) 583–598.
- [44] G.C. Chen, J.T. Yang, Two-point calibration of circular dichrometer with d-10-camphorsulfonic acid, *Anal. Lett.* 10 (1977) 1195–1207.
- [45] L. Whitmore, B.A. Wallace, DICHROWEB, an online server for protein secondary structure analyses from circular dichroism spectroscopy data, *Nucleic Acids Res.* 32 (2004) W668–W673.
- [46] L. Whitmore, B.A. Wallace, Protein secondary structure analyses from circular dichroism spectroscopy: methods and reference databases, *Biopolymers* 89 (2008) 392–400.
- [47] L.A. Compton, W.C. Johnson Jr., Analysis of protein circular dichroism spectra for secondary structure using a simple matrix multiplication, *Anal. Biochem.* 155 (1986) 155–167.
- [48] A. Abdul-Gader, A.J. Miles, B.A. Wallace, A reference dataset for the analyses of membrane protein secondary structures and transmembrane residues using circular dichroism spectroscopy, *Bioinformatics* 27 (2011) 1630–1636.
- [49] S. Haldar, A. Chaudhuri, A. Chattopadhyay, Organization and dynamics of membrane probes and proteins utilizing the red edge excitation shift, *J. Phys. Chem. B* 115 (2011) 5693–5706.
- [50] A. Chattopadhyay, S. Haldar, Dynamic insight into protein structure utilizing red-edge excitation shift, *Acc. Chem. Res.* 47 (2014) 12–19.
- [51] A.P. Demchenko, Site-selective red-edge effects, *Methods Enzymol.* 450 (2008) 59–78.
- [52] S. Mukherjee, A. Chattopadhyay, Wavelength-selective fluorescence as a novel tool to study organization and dynamics in complex biological systems, *J. Fluoresc.* 5 (1995) 237–246.
- [53] S. Guha, S.S. Rawat, A. Chattopadhyay, B. Bhattacharyya, Tubulin conformation and dynamics: a red edge excitation shift study, *Biochemistry* 35 (1996) 13426–13433.
- [54] S. Mukherjee, A. Chattopadhyay, Motionally restricted tryptophan environments at the peptide-lipid interface of gramicidin channels, *Biochemistry* 33 (1994) 5089–5097.
- [55] F.G. Prendergast, Time-resolved fluorescence techniques: methods and applications in biology, *Curr. Opin. Struct. Biol.* 1 (1991) 1054–1059.
- [56] A. Varrault, D.L. Nguyen, S. McClue, B. Harris, P. Jouin, J. Bockeaert, 5-Hydroxytryptamine_{1A} receptor synthetic peptides. Mechanisms of adenylate cyclase inhibition, *J. Biol. Chem.* 269 (1994) 16720–16725.
- [57] M.R. Eftink, L.A. Selvidge, P.R. Callis, A.A. Rehms, Photophysics of indole derivatives: experimental resolution of L_a and L_b transitions and comparison with theory, *J. Phys. Chem.* 94 (1990) 3469–3479.
- [58] A.J. Venkatakrisnan, T. Flock, D.E. Prado, M.E. Oates, J. Gough, M.M. Babu, Structured and disordered facets of the GPCR fold, *Curr. Opin. Struct. Biol.* 27 (2014) 129–137.
- [59] J.F.P. Dass, C. Sudandiradoss, The function and structural influence of selective relaxed constraint at functional intracellular loop₃ of 5-HT_{1A} serotonin-1 receptor family, *Gene* 508 (2011) 211–220.
- [60] J.R. Raymond, Y.V. Mukhin, T.W. Gettys, M.N. Garnovskaya, The recombinant 5-HT_{1A} receptor: G protein coupling and signaling pathways, *Br. J. Pharmacol.* 127 (1999) 1751–1764.
- [61] H. Chakraborty, A. Chattopadhyay, Sensing tryptophan microenvironment of amyloid protein utilizing wavelength-selective fluorescence approach, *J. Fluoresc.* 27 (2017) 1995–2000.
- [62] A. Chattopadhyay, S.S. Rawat, D.A. Kelkar, S. Ray, A. Chakrabarti, Organization and dynamics of tryptophan residues in erythroid spectrin: novel structural features of denatured spectrin revealed by the wavelength-selective fluorescence approach, *Protein Sci.* 12 (2003) 2389–2403.
- [63] A. Chaudhuri, S. Haldar, A. Chattopadhyay, Organization and dynamics of tryptophans in the molten globule state of bovine α -lactalbumin utilizing wavelength-selective fluorescence approach: comparisons with native and denatured states, *Biochem. Biophys. Res. Commun.* 394 (2010) 1082–1086.
- [64] D.A. Kelkar, A. Chaudhuri, S. Haldar, A. Chattopadhyay, Exploring tryptophan dynamics in acid-induced molten globule state of bovine α -lactalbumin: a wavelength-selective fluorescence approach, *Eur. Biophys. J.* 39 (2010) 1453–1463.
- [65] M. Mitra, A. Chaudhuri, M. Patra, C. Mukhopadhyay, A. Chakrabarti, A. Chattopadhyay, Organization and dynamics of tryptophan residues in brain spectrin: novel insight into conformational flexibility, *J. Fluoresc.* 25 (2015) 707–717.